Journal of The Electrochemical Society, 2022 **169** 120528

Experimental Study of Sidewall Rupture of Cylindrical Lithium-Ion Batteries under Radial Nail Penetration

Haodong Chen,[1,z] Evangelos Kalamaras,[1,2] Ahmed Abaza,[3] Yashraj Tripathy,[1,2] Jason Page,[3] and Anup Barai[1,z]

[1]*WMG, University of Warwick, Coventry CV4 7AL, United Kingdom*
[2]*The Faraday Institution, Harwell Campus, Didcot OX11 0RA, United Kingdom*
[3]*Jaguar Land Rover Limited, Whitley, Coventry CV3 4LF, United Kingdom*

To understand the relationship of the sidewall rupture at different states of charge (SOCs) of cylindrical cells with high specific energy, this work presents the results of radial nail penetration tests of 21700-format cylindrical cells at different SOCs. The thermal runaway and sidewall rupture behaviours were characterised by key performance indicators such as temperature, mass, fire behaviour, and voltage change. In addition, released gases from a subset of tests were measured using the Fourier transform infrared spectroscopy. The change in the internal structure of another subset of cells after the test was observed by X-ray computed tomography. The results show that the sidewall rupture still exists for tests at low SOC ($< 30\%$ SOC), but the outcome of thermal runaway and sidewall rupture is milder than those at high SOC ($\geqslant 50\%$ SOC). The average mass loss of cells increases with the increment of SOC. The cell casing thickness is reduced by $12.7\% \pm 0.3\%$ of the fresh cell, which in combination with the reduction in the strength of the casing material at high temperatures could contribute to sidewall rupture.

 [DOI: 10.1149/1945-7111/acadac]

Manuscript submitted October 3, 2022; revised manuscript received November 25, 2022. Published December 30, 2022.

Supplementary material for this article is available online

In recent years, there has been a lot of news about electric vehicle (EV) battery fire.[1] Although such events rarely led to fatal incidents, the root cause of such failures in real-world applications has not been completely understood by the scientific community. Such events are mainly initiated by thermal runaway (TR) of a lithium-ion battery (LIB) cell, which can be triggered under abuse conditions, e.g. accidents or LIBs with manufacturing defects.[2,3] Energy released from a cell TR may damage adjacent cells or even cause the adjacent cells to TR, known as TR propagation.[4–15]

Many kinds of battery abuse conditions, categorised as electrical, mechanical, thermal, and environmental can lead to cell TR.[16] The outcome of cell TR ranges from the release of toxic and non-toxic gases, smoke, spark, fire, rupture or explosion.[2,3] Rupture is one of the most severe scenarios of battery failure and it happens when stresses generated by internal pressure and thermal strain exceed the strength of the battery casing itself. Once one or more cells have sidewall rupture, sparks, hot gases, and flames coming out from the opening of the cell side can promote cascading failure of adjacent cells.[8,12,13] To prevent rupture or explosion, the vent disk is designed to relieve internal pressure caused by generated gases inside the cell when reaching its critical pressure.[8,17] However, the vent disk is sometimes partly or completely blocked by the electrode assembly or not activated due to malfunction even when the internal pressure has exceeded its critical pressure.[17,18]

The sidewall rupture behaviour of LIBs under abuse conditions has been reported recently.[8,18–22] Anderson et al.[19] investigated the risk of sidewall ruptures of 18650-format cells during oven heating and found that both cells with a thin can or casing and volumetric energy density of higher than 660 Wh l^{-1} have a high likelihood of sidewall rupture. But there is very limited information about sidewall rupture behaviour in their presentation. Finegan et al.[18,20] characterized the venting processes of commonly used commercial 18650-format cells during TR triggered by external heating. The dynamic processes of TR propagation within cells were observed via a high-speed X-ray computed tomography (CT) and the venting mechanisms of different 18650-format cells were analysed. Adding a base vent was found to be an effective way to greatly reduce the risk of cell rupture for the following tests of 18650-format cells with a base vent.[18] Their study concludes that the vent is not enough for gases to flow out as it is blocked by the electrode assembly, which is the leading cause of cell rupture. Kong et al.[21] also found that casing rupture was caused by blockage of the venting region after conducting a post-mortem analysis of a 18650-format cell and two 20700-format cells via X-ray CT. The rupture in 21700-format cells during TR triggered by external heating was also reported by Lao et al.[8] Their tests demonstrate that a decrease in mechanical strength at high temperatures is one of the key factors that can lead to sidewall rupture or tear crack. In addition, Zhu et al.[22] observed the rupture of prismatic cells under overcharge and found that casing rupture time decreased with the increase of charge rate from 1C to 5C under overcharge due to more Joule heat generated under large current.

As can be seen, the previous studies mostly focused on the understanding of TR mechanism and rupture behaviour of LIBs with lower specific energy such as 18650-format cells. However, detailed relationship between sidewall rupture and SOC has never been reported. In addition, dependency of the rupture and fire behaviours on SOC has never been established. The work reported here aims to address this knowledge gap. With the increased specific energy of the cell, achieved exploiting high nickel content within the active material increases the risk of sidewall rupture. Therefore, the research presented here is timely, and of value to the research community.

Experimental

To investigate the sidewall rupture behaviour of the high specific energy cells at different SOCs, this work adopted nail penetration test because it is one of the mechanical abuse tests and is widely adopted to evaluate the risk of TR of LIBs and to act as a trigger of TR initiation.[23–29] In addition, compared to external heating abuse and overcharge abuse conditions, nail penetration tests do not introduce additional energy to the cell. Therefore, in this work, a series of nail penetration tests was performed on 21700-format cells with a high specific energy and different SOCs. Some key parameters including temperature, mass, fire behaviour, and voltage were recorded in tests to characterise the TR and sidewall rupture behaviours. In addition, released gases in some tests were measured using a Fourier transform infrared spectroscopy (FTIR) and the internal structure of two cells with 100% SOC was observed by X-ray computed tomography (CT).

[z]E-mail: Haodong.chen@warwick.ac.uk; a.barai@warwick.ac.uk

Table I. Battery information.

Item	Specification
Format	21700
Rated capacity	4.8 Ah
Nominal voltage	3.62 V
Charge cut-off voltage	4.2 V
Discharge cut-off voltage	2.5 V
Mass	67.5 g ± 1.5 g
Cathode	Lithium nickel cobalt aluminium oxide
Anode	Graphite and Si

Battery sample.—The commercial cylindrical 21700-format LIBs with the specific energy of 257 W·h kg^{-1} were used in this work and the battery information from the manufacturer is listed in Table I. All cells were discharged to the desired SOC, ranging from 20% to 100%, with 1C (4.8 A) discharging rate before the tests and rested for at least 1 h. The lowest SOC of 20% was selected as all the tests at this SOC expected not to initiate sidewall rupture.

Measurement setup.—A schematic diagram of the experimental setup is shown in Fig. 1. The cell without its plastic envelope was fixed by a cell holder made of Tufnol material using screws and nuts and the cell holder was clamped on a steel plate by G-shape jigs. Temperatures on the cell surface were measured by three K-type thermocouples with the accuracy of ±1.5 °C, which were located at 10 mm from the cell base, in the middle of the cell, and 10 mm from the cell top, respectively, and temperatures were recorded by a data logging software (PicoLog, UK) with a time interval of 10 ms. One infrared radiation (IR) camera (FLIR T640, USA) positioned at a stand-off distance of 1.52 m from the back of the cell and recording at 30 frames per second was used to capture temperature evolution on the cell surface. Two high definition (HD) cameras recording at 30 frames per second were in the front of the cell with 0.72 m and the side of the cell with 0.44 m, respectively, to capture the TR and rupture behaviours during the test. As shown in Fig. 1, one HD camera and the IR camera are set-up directly facing the cell and the other HD camera is on the side of the cell. The Fourier transform infrared (FTIR) (Gasmet, UK) gas analyser was used to perform the real-time analysis of released gas components during TR. The location of the inlet hole was about 4 cm diagonally above the cell.

Nail parameters.—For the penetration, the nail was made of stainless steel with a conical of 40° and a diameter of 4 mm and a length of 54 mm. Penetration was done at a speed of 6 mm s^{-1} controlled by the hydraulic nail penetration system (Torishima, UK). These nail penetration parameters were adopted as they are suggested by a number of international and national standards such as GB 38031–2020. The activity of nail penetration was stopped when cells were triggered to TR, that is, the nail was no longer going further inside the cells when sparks ejected from cells were observed as a condition that TR occurred in this work. A selected number of cells were scanned by X-ray CT before and after the test to observe the internal structure changes.

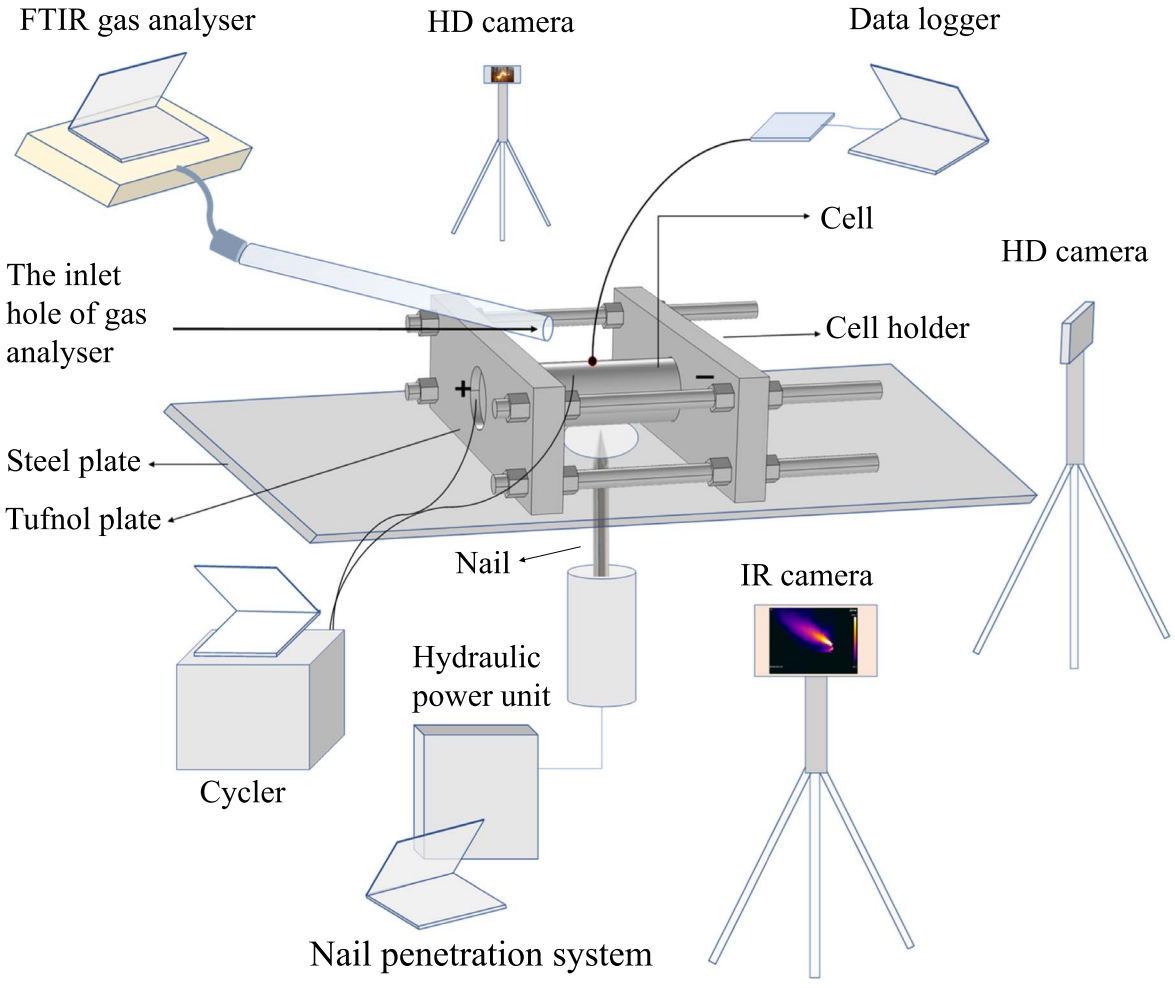

Figure 1. Schematic diagram of the test apparatus.

Results and Discussion

A total of 21 tests were conducted: six tests of them with 100% SOC and the rest with other SOCs. Considering test repeatability, six tests were performed at 100% SOC due to the failure of test no. 5 in recording temperatures. For tests at other SOCs, we aimed to determine the minimum SOC that could cause sidewall rupture. Two tests were performed at each condition between 25% SOC and 70% SOC, and five tests were performed at 20% SOC for test repeatability as there was no sidewall rupture at 20% SOC in this work. Table II lists testing conditions and a summary of the maximum temperature on the cell surface during the test. TR happened in 16 tests while five tests at low SOC did not go into TR. It happened easier for tests at high SOC as reported by previous researchers using other cells[25,30] because there is more heat generated at high SOC cells during nail penetration. Figure 2 presents photos of tests 1–18 after the test, photos of tests 19–21 do not show here because they are similar with tests 17 and 18, see Fig. S1.

As shown in Table II and Fig. 2, sidewall rupture is with TR in most of them but only one test at 25% SOC without TR. For cells at 50% SOC or higher, sidewall rupture was observed in all tests including one with 100% SOC showing holes created by melting the metallic casing. Sidewall rupture was also found in tests less than 50% SOC. One of two tests at SOC from 25% to 40% happened sidewall rupture. As expected, sidewall rupture was not observed in tests when the cell SOC was further reduced. The rupture behaviour of tests at 70% SOC was similar to that at 100% SOC with a relatively small opening. The vent disk was believed to activate before sidewall rupture because the sparks or fire were observed ejecting from venting holes ahead of that from the cell side. Some catastrophic explosion cases were observed in tests less than 70% SOC and their ruptures propagated through the penetrating location maybe because the vent disk was completely or partially blocked, and the strength of the casing around the penetrating hole was less than the original strength due to a deep insertion for lower SOC, therefore the penetrating location became the weak point of the casing. The opening of the penetrating location looked bigger than the nail diameter for tests less than 100% SOC with TR because sparks were also ejected from the penetrating location in these tests and therefore increased the opening area. Note that the penetrating depths of tests at 100% SOC were shallower than those with low SOC because the tests were stopped with the observation of sparks and the tests at 100% SOC were easier triggered to TR than those at low SOC. The occurrence of catastrophic explosion for tests at low SOC suggests that insertion depth is also a contributing factor to sidewall rupture and the deep insertion may facilitate the violent sidewall rupture. The present results show that the increase of SOC greatly increases the likelihood of sidewall rupture. The main reason is that the internal pressure generated by gases released during TR is very high and the strength of the battery casing greatly degrades at high temperatures.[8] In addition, the structural integrity of the cell may be damaged by the impulse force generated by the nail during penetration, see test 16 with 25% SOC and without TR. Further analysis of sidewall rupture will be done by comparing mass after test, gas released, and CT scan in the following sections.

Temperature analysis.—As shown in Table II, the maximum surface temperature of the cell in some tests exceeds 800 °C, which is close to the internal maximum temperature, 820 °C, measured by an embedded thermocouple in a similar nail penetration test with an 18650-format cell[31] and is higher than that reported in nail penetration tests using other 18650-format cells.[25] In addition, some molten balls of aluminium foil were observed in some tests, confirming that the internal temperature did exceed 660 °C (melting point of aluminium foil). It shows that the outcome of TR of the current 21700-format cells is more severe than 18650-format cells. The mean value of maximum surface temperature and its standard deviation are shown in Fig. 3. The average of the maximum surface temperature located at 10 mm from the cell base (negative terminal) decreases with the decrease of SOC. The mean value of maximum surface temperature in tests at 20% SOC and 25% SOC are not plotted here due to one test with TR while the other without. Overall, it shows a trend of reduction in the average maximum surface temperature with SOC decrease. Figure 4 presents temperature profiles at different locations of 100% SOC cells. The temperature rises to the maximum in a few seconds, then decreases gradually due to cooling. The temperature drop for Test 4 in Fig. 4b is likely due to poor contact during the test. Note that temperatures in test 5 are not presented here because thermocouples fell off the cell surface during the test.

Fire behaviour.—As shown in Fig. 5, some key images from test 1, as a representative example, are extracted to present the fire

Table II. Summary of the experimental results.

SOC	Test No.	10 mm from top (°C)	Middle (°C)	10 mm from bottom (°C)	Thermal runaway	Sidewall rupture
100%	1	683.97	—	746.17	Yes	Yes
	2	862.42	802.84	713.96	Yes	Yes, melting holes
	3	673.41	646.50	821.32	Yes	Yes
	4	684.59	641.15	761.82	Yes	Yes
	5	—	—	—	Yes	Yes
	6	831.76	756.31	860.40	Yes	Yes
70%	7	692.71	715.42	719.82	Yes	Yes
	8	768.02	1073.05	791.98	Yes	Yes
50%	9	620.78	784.68	719.82	Yes	Yes
	10	618.81	751.62	539.11	Yes	Yes
40%	11	618.71	679.6	542.94	Yes	No
	12	624.93	—	581.41	Yes	Yes
30%	13	450.74	614.59	347.63	Yes	Yes
	14	534.68	647.16	494.64	Yes	No
25%	15	570.74	597.11	579.97	Yes	No
	16	133.5	146.47	140.04	No	Yes
20%	17	553.19	604.12	549.17	Yes	No
	18	143.15	162.30	158.89	No	No
	19	150.43	160.61	155.49	No	No
	20	140.01	147.79	137.82	No	No
	21	148.21	156.66	153.56	No	No

Figure 2. Photos of tests 1–18 after the test.

characteristic of tests at 100% SOC. Here the time is set to be zero when sparks were observed in tests. Smoke and sparks ejected together from venting holes at the initial stage of TR, followed by a burst of sparks and flames from venting holes, and then flames burst from the side of the cell, next, the fire was extinguished after consumption of all combustible gases and finally, the cell cooled down. There was no great difference between different tests at 100% SOC. The whole process could be mainly divided into three stages: spark, flame and cooling. In the stage of spark, a large number of sparks with smoke ejected firstly from venting holes, and then also from the opening of the cell side (sidewall rupture) within 1 s. Many bursts of sparks from venting holes and the opening of the cell side were observed in this stage, while a very weak ejection of sparks was from the penetrating location. It suggests that the pressure valve works when the internal pressure exceeds its critical value. Sidewall rupture occurring at this stage also suggests that the internal pressure is extremely high, and the opening area of the valve is not large enough to release pressure in such a short time. The smoke here

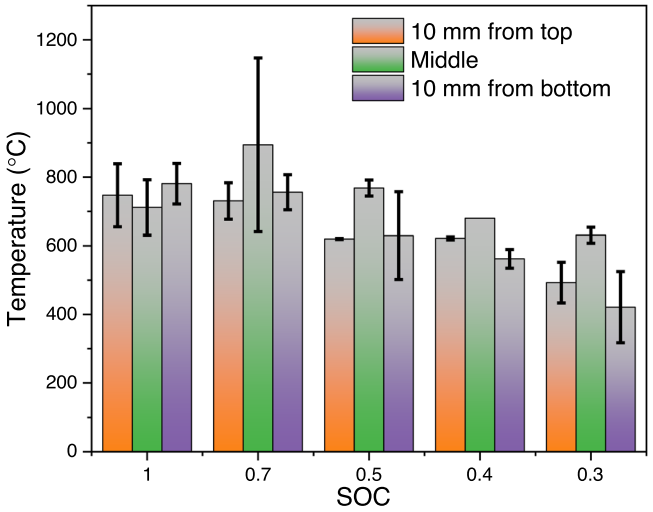

Figure 3. Average maximum surface temperature of cells at different SOCs.

mainly consisted of electrolyte vapours, carbon dioxide and water vapour because the concentration of these gases increased quickly at this stage, see more results about gases analysis in the following section. The concentration of these gases should be beyond the flammability limits of the gas mixture because these gases were not ignited by sparks.[32] In the stage of flame, jet fire ejected from both venting holes and the opening of the cell side until the fire extinguished for exhausting all combustible gases, and many fragments ejected before forming the steady jet fire. There was an overlap between the stages of sparks and flame. The sparks were dominated in the stage of spark and the jet fire was dominated in the stage of flame accordingly. The transition from sparks to jet fire had been discussed in detail in our previous study of cylindrical cells with external heating using a high-speed camera.[32] The cell cooled down gradually to room temperature in the stage of cooling. According to the definition, the first two images in Figs. 5a–5b are in the stage of sparks, the third image and the fourth image are in the stage of transition and the fifth image is in the stage of flame, and the last one is in the stage of cooling. The temperature distribution of the whole cell and the TR characteristics were also captured by the IR camera as shown in Fig. 5c.

The fire behaviour of cells at low SOC is not the same as with 100% SOC. It needs to be analysed one by one. For test 7 at 70% SOC (shown in Figs. S2a and S2b in supplementary material), a very small number of sparks with low brightness were firstly ejected from venting holes, then a flame was ejected from venting holes after 0.03 s, shortly afterwards, sparks were ejected from venting holes as well as from the opening of the side, finally, a small jet fire was observed from the opening of the side. TR propagation within the cell was observed initially from the penetrating location to two ends of the cell in the longitudinal direction and then in the radial direction of the cell via the IR camera (see Fig. S2c in supplementary material), and the whole process of TR propagation lasted for about 1 s. The fire behaviour of test 8 at 70% SOC is similar to that at 100% SOC.

For test 9 at 50% SOC (shown in Fig. S3 in supplementary material), sparks ejected from the penetrating location, then from the opening of the side. There were no sparks ejected from venting holes. The violent jet fire was mainly observed from the opening and a small part of it from venting holes due to a large opening of the cell side. For test 10 at 50% SOC, sparks and flame were only ejected from the opening of the side, and a lot of white smoke was released from venting holes during the test.

For test 11 at 40% SOC without sidewall rupture (shown in Fig. S4 in supplementary material), some sparks were firstly ejected from the penetrating location, then some smoke was released from venting holes, next some sparks were ejected from venting holes with smoke,

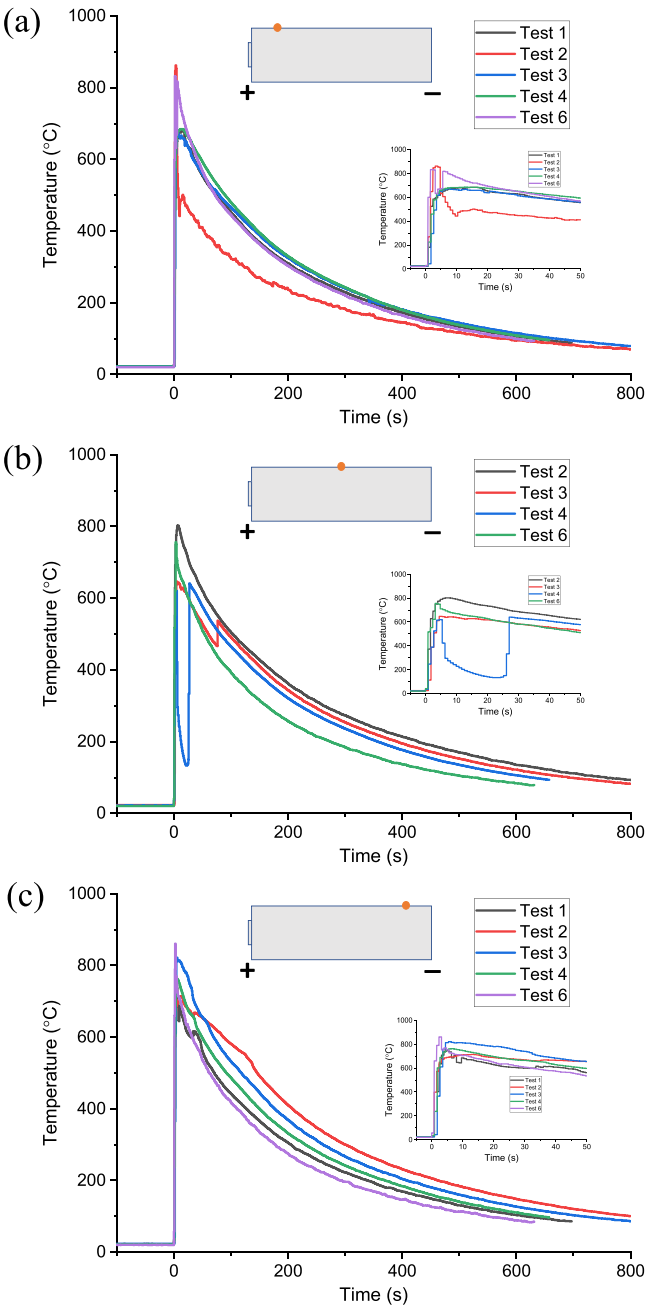

Figure 4. Temperature profiles at different locations of 100% SOC cells. (a) 10 mm from the cell top, (b) middle of the cell, and (c) 10 mm from the cell base.

after that some cyan blue smoke and many white gases were released from venting holes and lasted for about 10 s. The flame was not observed in this test. For test 12 at 40% SOC with sidewall rupture, smoke, sparks and flame were not observed ejecting from venting holes, but a large flame burst from the opening of the side, lasting only for less than 1 s.

For test 13 at 30% SOC with sidewall rupture (shown in Fig. S5 in supplementary material), there was a lot of smoke from the side of the cell during the test, whereas flame was not observed in this test. For test 14 at 30% SOC without sidewall rupture, a lot of white smoke was released from venting holes. The flame was not observed either. For test 15 at 25% SOC without sidewall rupture, some sparks were observed ejecting from the penetrating location, and then a lot of white smoke was released from venting holes. For test 16 at 25% SOC with sidewall rupture shown in Fig. S6

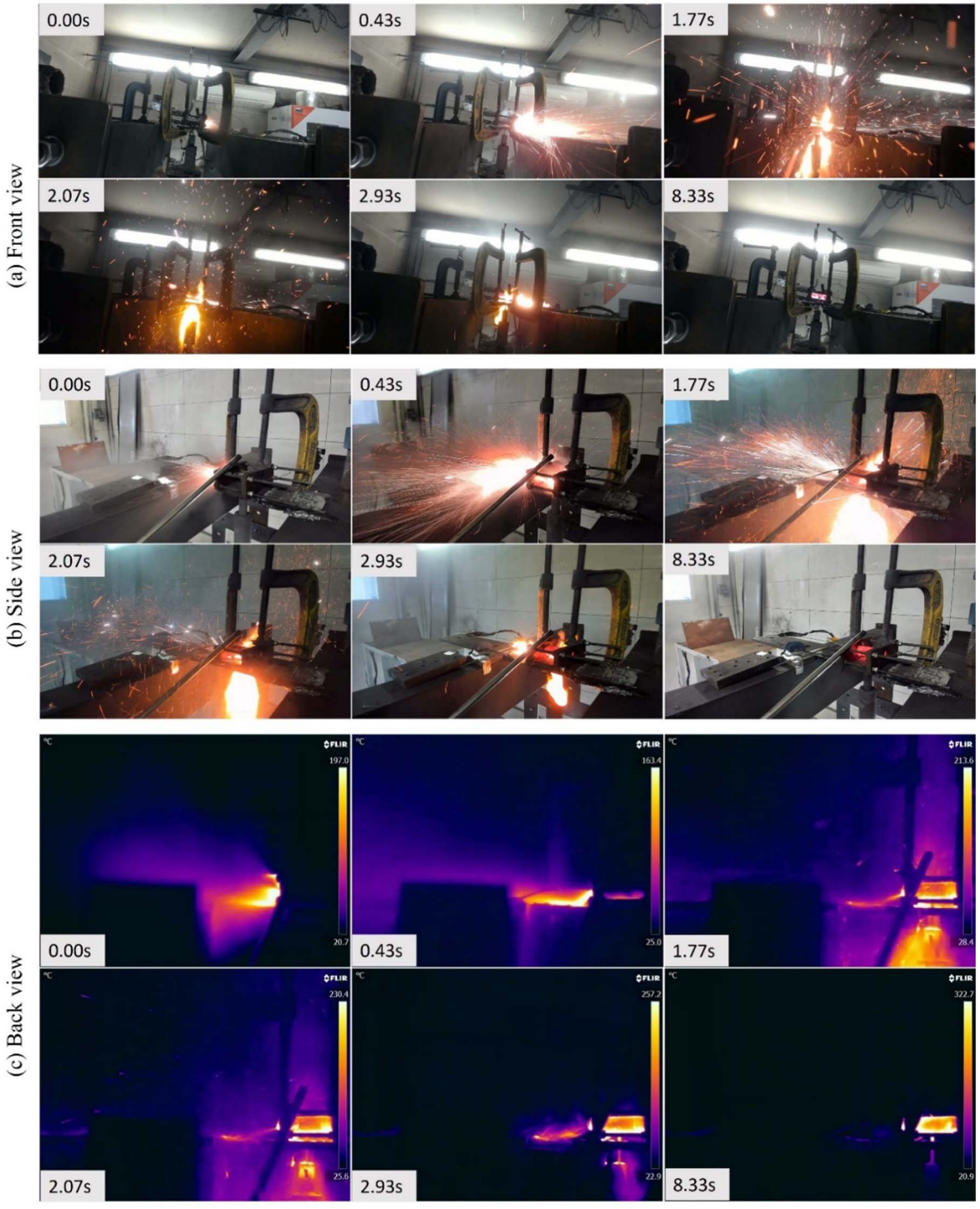

Figure 5. Evolution of fire behaviour of test 1 at 100% SOC. (a) Front view, (b) side view, and (c) back view from the IR camera.

(supplementary material), sparks were only observed during penetration, and a small amount of smoke was released from the cell side. Although the sparks were observed, the temperature of the cell did not reach very high, only up to 146.47 °C, and it suggests that the cell did not go into TR. The phenomenon of test 17 at 20% SOC is similar to test 15 at 25% SOC. There was only a small amount of smoke released from the penetrating location with tests 18–21 at 20% SOC.

In general, as reported in earlier research, cells at high SOC went into TR easier than those at low SOC.[25] A violent burst of sparks and flame and a small amount of smoke were released for cells greater than or equal to 50% SOC, whereas many gases were released, and a small number of sparks ejected and no flame for cells both less than 40% SOC and with TR. There were only some smoke and a very small number of sparks and no ejection for tests without TR.

Mass and voltage analysis.—Figure 6a presents the average mass of cells after the test decreases with the increase of SOC, which is consistent with the trend of change in average maximum surface temperature with SOC. There is a lot of Joule heat generated by an internal short circuit during nail penetration, then followed by a series of overlapped and temperature-dependent exothermic

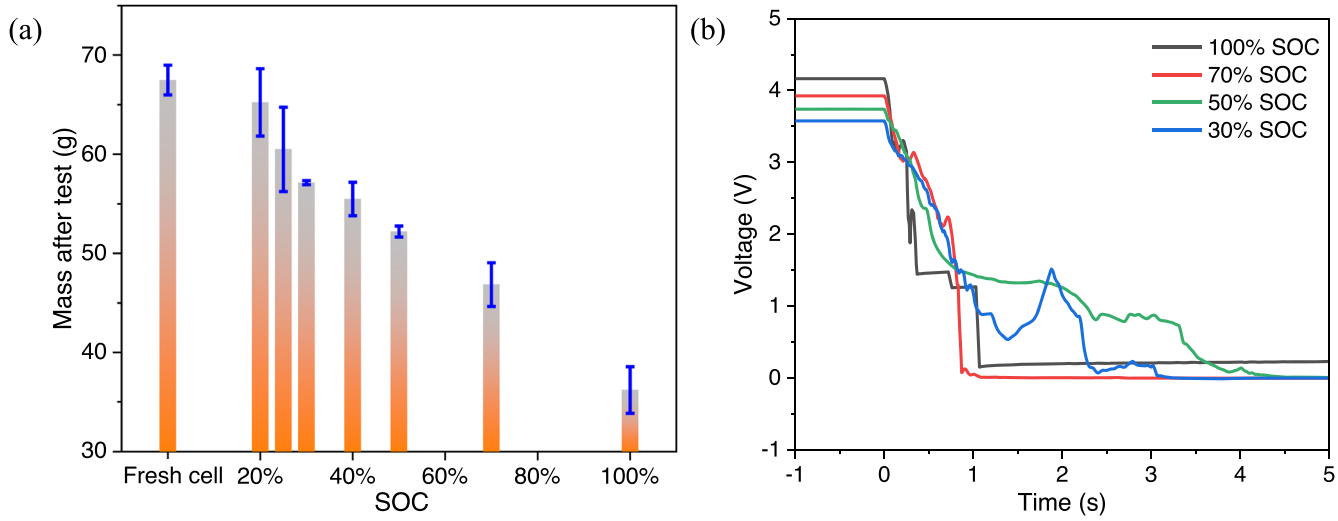

Figure 6. (a) Average mass of cell after test at different SOCs, and (b) Cell voltage profile during test at 100% SOC (test 6), 70% SOC (test 8), 50% SOC (test 10), and 30% SOC (test 14).

reactions, which mainly consists of solid electrolyte interphase (SEI) decomposition, the reaction of electrolyte with anode/cathode material and binder, cathode material decomposition, and electrolyte decomposition.[2,3,33] Cells retained about 53.7% of original mass after the test at 100% SOC and 96.7% for tests at 20% SOC. It suggests that more battery components are ejected for cells at high SOC during TR. The possible reasons for the tests at 100% SOC suffering more cell mass loss but less sidewall rupture severity are as follows: (1) the internal pressure generated inside the cell at 100% SOC is larger than other SOCs due to more energy stored in the cell, and therefore more gas and energy are released after nail penetration, which increases the internal pressure and therefore more battery components and gas are ejected from the cell under high internal pressure. (2) As shown in Fig. 2, the insertion depth for tests at 100% SOC is shallower than low SOCs, therefore, the strength of the casing around the penetrating hole is less influenced than tests at low SOC with a deep insertion. As described above on fire behaviour, the videos also showed a more violent burst of sparks and flame for tests at high SOC and only gases for those tests at low SOC. The present results further confirm that the outcome of TR for cells at high SOC is more severe than for those at low SOC.

The voltages of part cells in the test were recorded using a cycler (Maccor, USA). The interval of data sampling is 0.01 s. As shown in Fig. 6b, the voltage of the cell drops until close to 0 V during nail penetration because a hard short circuit happens after the nail is inserted into the cell. The voltage dropped quickly for cell at high SOC due to the larger initial open circuit voltage and the small shorting resistance, which changed with time during nail penetration. Sharp voltage changes mean more Joule heating generated and more violent reactions happened in the cell during nail penetration.

Gases analysis.—The released gas components during TR were analysed via the Fourier transform infrared spectroscopy (FTIR) gas analyser. In these tests, the cell was in an open environment and the sampling inlet kept the same location about 4 cm diagonally above the nail penetration position. As shown in Fig. 7, carbon dioxide (CO_2), water vapour (H_2O), carbon monoxide (CO), nitrogen monoxide (NO), nitrogen dioxide (NO_2), hydrogen chloride (HCl), methane (CH_4), ethane (C_2H_6), ethylene (C_2H_4), hexane (C_6H_{14}), formaldehyde (CHOH), ethylene carbonate ($C_3H_4O_3$), dimethyl carbonate ($C_3H_6O_3$), and ethyl methyl carbonate ($C_4H_8O_3$) were detected in tests. These gases were products of exothermic reactions such as electrolyte decomposition and the reaction of electrolytes with anode/cathode material.[2,3] Carbon dioxide had the greatest concentration of all the detected gases. The high concentration of CO_2 was mainly attributed to the combustion of released gases and graphite.[34] The concentration of CO_2 in tests with 100% SOC was lower than that with other SOCs, which may be because the opening of the cell side is smaller than in tests with lower SOCs and therefore more CO_2 ejects from the venting holes for 100% SOC tests. The water vapour had the second greatest concentration of all the detected gases, and the next was CO. As shown in Figs. 7c–7f, concentrations of other detected gases are lower than the concentration of CO and the maximum concentration of them is less than 500 ppm. $C_3H_4O_3$, $C_3H_6O_3$ and $C_4H_8O_3$ have commonly used electrolyte solvents, which are detected in the test, indicating that they are adopted in this cell. Hydrogen (H_2) was commonly reported in other Refs. 34–36 but not showing here due to a missing H_2 sensor in the equipment used for this experiment.

Note that the concentration of measured gas depends not only on the SOC but also on the opening on the cell side. Large openings will release more gases than the venting holes. Due to the open environment in these tests, the concentration of measured gas is also dependent on where the inlet hole of the gas analyser is placed. In addition, there are many other factors influencing the measured gas concentrations such as humidity.[23] For example, an increase in the humidity in the surrounding atmosphere led to a reduction of measured gas concentrations during TR because some gases dissolved into water and some of them condensed easily on the chamber surface.[23]

X-ray CT analysis.—The X-ray CT being a non-destructive method was also used to observe the internal structure during TR.[21,27,31,37,38] In this work, two cells (test 2 and 3) at 100% SOC after the test and one fresh cell at 0% SOC were scanned by the X-ray CT (Zeiss Metrotom 1500, Germany) with an exposure voltage of 200 kV, an exposure power of 39.2 W, and an exposure time of 1 s to generate 3000 projections with a voxel size of 31 μm. Software (MetrotomOS and VG Studio Max 2.2, Germany) was used to reconstruct the individual radiographic scans.

Figure 8 presents the internal structure of the fresh cell. Figures 8a and 8b are cross-section images in the longitudinal direction and the radial direction, respectively. The part with higher density displays brighter or has a higher greyscale value because the material with higher density has more X-ray absorption,[39] and therefore battery casing, current collectors, cathode material and tabs display brighter and anode material, seal insulator, and void show darker. As shown in Fig. 8a, the anode is longer than the

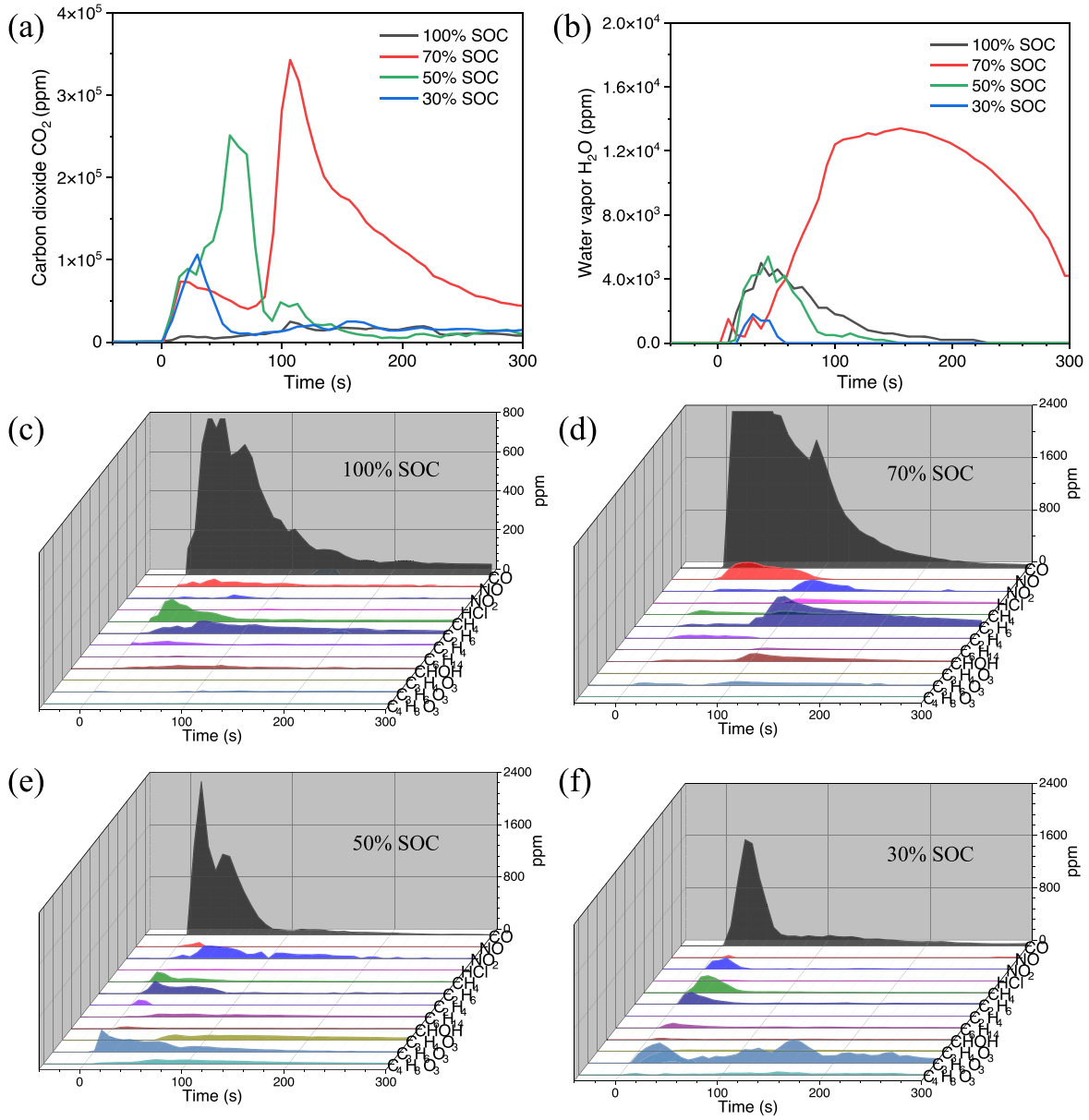

Figure 7. Concentration of (a) carbon dioxide and (b) water vapor in tests at 100% SOC (test 6), 70% SOC (test 8), 50% SOC (test 10), and 30% SOC (test 14), and concentration of different gases in tests with test 6 (c), test 8 (d), test 10 (e), and test 14 (f).

cathode, which is commonly used in battery design. There are a total of 27 windings according to the number of positive electrode layers. In addition, there is no mandrel in this cell.

Figures 9a–9d and 9e–9i present slice images of test 2 at 100% SOC in the longitudinal direction at different angles and the radial direction at different heights from the cell base to the cell top, respectively. The visual image of this cell is shown in Fig. 2. As shown in Fig. 9, many metal particles are spreading all over electrode materials, and there is a big cavity located in the lower part of the cell with a volume of about 2400 mm^3. The electrode materials close to the centre of the cell were severely damaged and moved forward to venting holes with the pushing force caused by ejecting sparks and jet fire. However, the electrode materials between the battery casing and the electrode layer connected to the negative tab were slightly damaged although the nail tip was in this region. The electrode layer connected to the negative tab could be considered as a boundary to distinguish the electrode materials badly damaged and those slightly damaged. The possible reasons are that the region with the electrode materials badly damaged easily moves towards the centre and venting holes than the rest part and positive feedback between temperature and chemical reaction is strong in this region due to no mandrel in the centre of the cell. The negative tab might be made of Ni[40] is intact and still connected to the battery base due to the higher melting point of Ni (1455 °C). There are two big melting holes, see Fig. 2, close to the penetrating location and two small melting holes between the penetrating location and the battery base. These holes were generated because part of the casing (melting point, >= 1375 °C) was melted under high temperature and acted as pathway for the release of gases and pressure during TR. It suggests that the internal temperature of the cell did reach over 1375 °C in this test. Cavities were observed around these holes and in other places without holes. All of them are connected directly or indirectly inside the cell. There are a lot of molten fragments attached to the inner case of the cell around venting holes and two big melting holes and the spin groove location as shown in Figs. 9a–9d and 9i. These fragments showed brighter

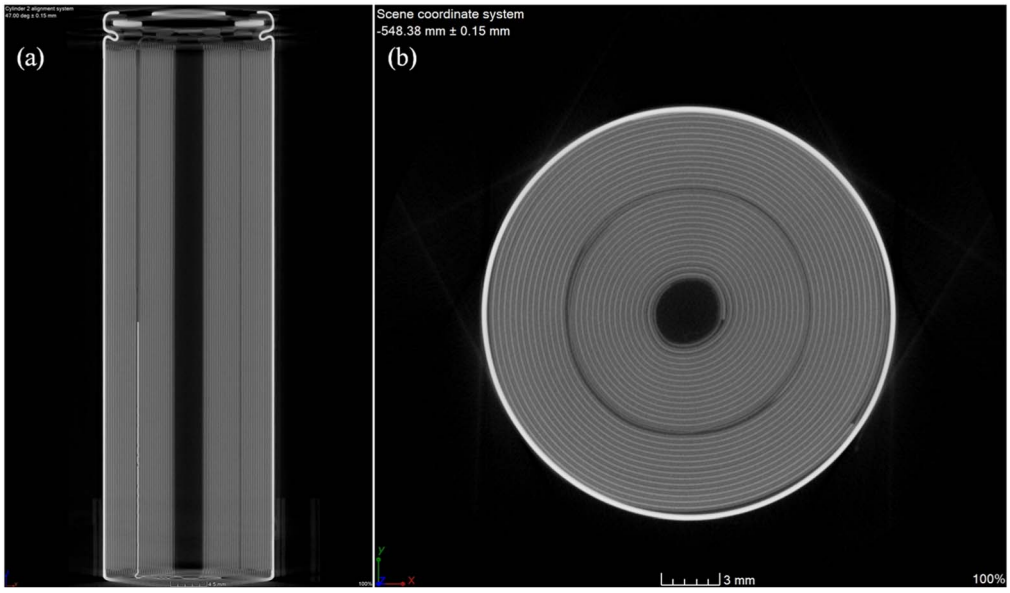

Figure 8. Internal structure of the fresh cell. Slice images in the longitudinal direction (a) and in the radial direction (b).

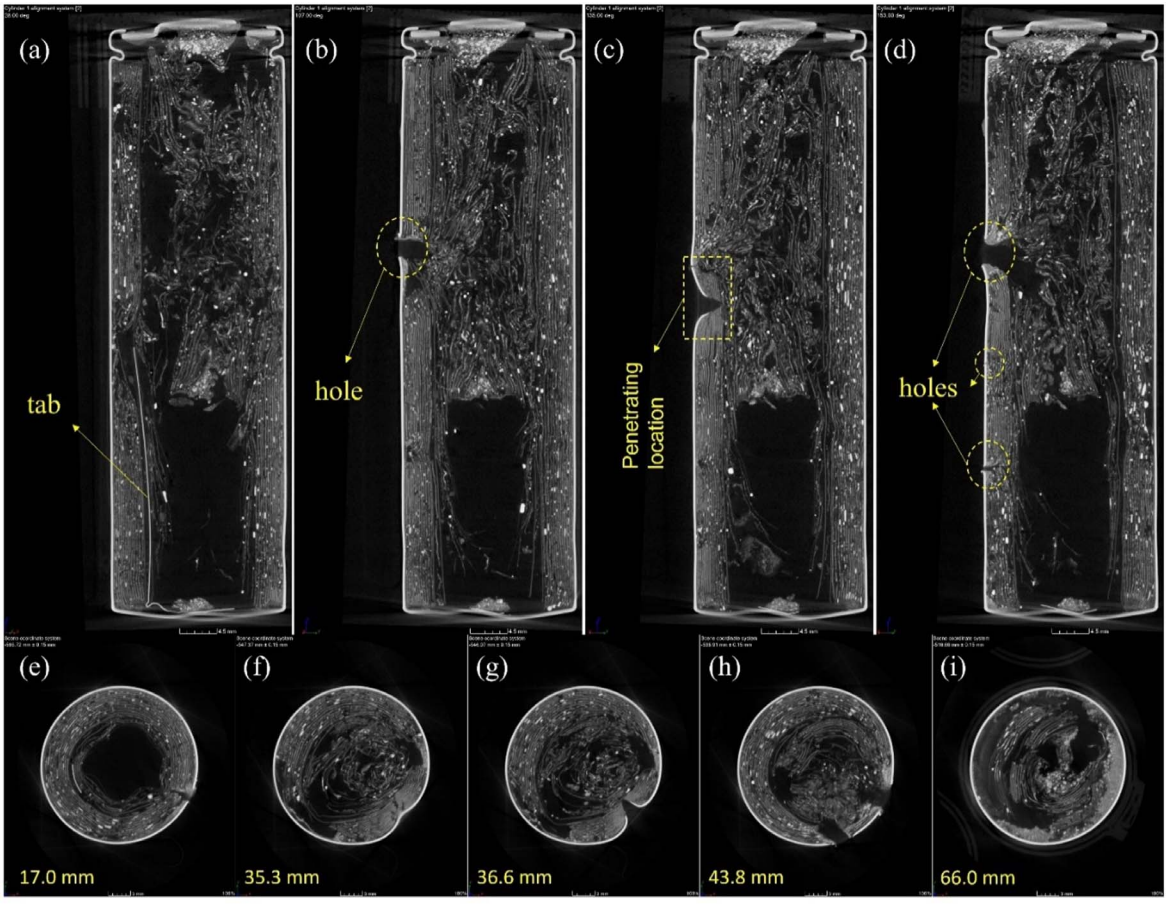

Figure 9. Internal structure of test 2 at 100% SOC. Slice images in the longitudinal direction at different angles (a)–(d) and in the radial direction at different heights (e)–(i) from the cell base to the cell top.

and were likely a mixture of metal and other products and mainly consisted of aluminium and products of the cathode material decomposed at high temperatures.

The dynamic process of TR propagation within 18650 cells under nail penetration was observed by Finegan et al.[31] via a high-speed synchrotron X-ray radiography, which gave some inspiration to analyse the process of TR in this test. During nail penetration, the battery casing was firstly punctured and followed by the damage to electrode assembly. Some cracks propagated in the radial direction along with the electrode assembly as shown in Fig. 9f may be due to

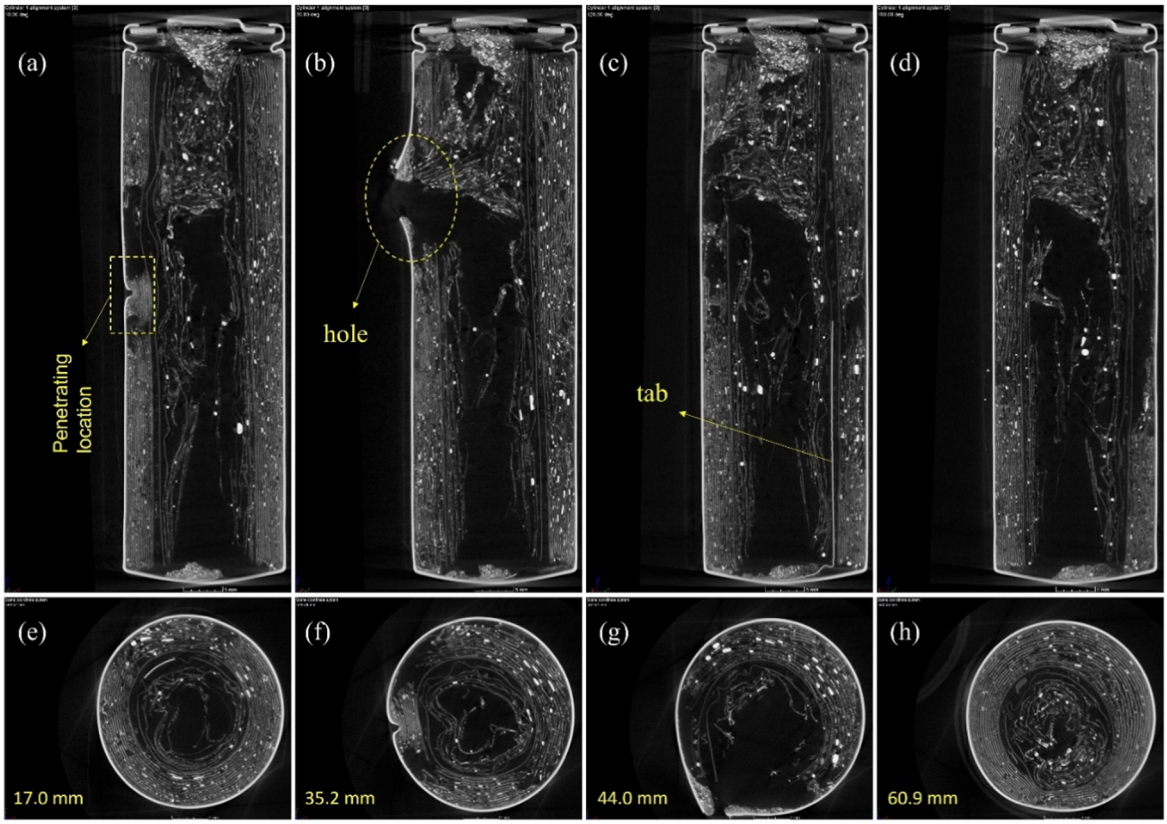

Figure 10. Internal structure of test 3 at 100% SOC. Slice images in the longitudinal direction at different angles (a)–(d) and in the radial direction at different heights (e)–(h) from the cell base to the cell top.

the tear force caused by the forward movement of the nail. Similar cracks were also reported by Finegan et al.[31] The cathode electrode and the anode electrode were contacted directly or by the nail during piercing the cell, and therefore internal short circuit occurred, and at the same time the cell started to discharge forcedly, and the voltage of the cell dropped rapidly as shown in Fig. 6b (same testing condition but not the same test).

The process of transport of electrons and lithium ions during an internal short circuit is as follows:[41] the electrons and lithium ions are released from the anode active material due to a delithiation reaction and at the same time the electrons are transport to the cathode active material and the aluminium current collector and the lithium ions transport through the separator to the cathode active material. A large amount of energy stored in the cell was released in a very short time due to the generation of a high current, which flowed through the cell and the short-circuited spot, and therefore the penetrating region of the cell was heated to a high temperature that may lead to a series of exothermic reactions and even to trigger the initiation of TR. In this test, the initiation of TR appeared to occur around the tip of the nail, and it propagated along with the longitudinal and azimuthal directions of electrode assembly relatively faster than that in the radial direction at the early stage.[31] The vacant core of the cell provided a space for the electrode assembly moving towards the centre. As shown in Fig. 9, the inner layers of electrode assembly bounded by the tab is in a state of disorder and the electrode materials are broken into pieces due to high temperature and high pressure. TR propagation within the cell was observed and initiated from the penetrating location to two ends of the cell in the longitudinal direction and then towards the rest part of the cell via the IR camera.

Figures 10a–10d and 10e–10i present slice images of test 3 at 100% SOC in the longitudinal direction at different angles and the radial direction at different heights from the cell base to the cell top, respectively. The depth of insertion of this test is shallower than that

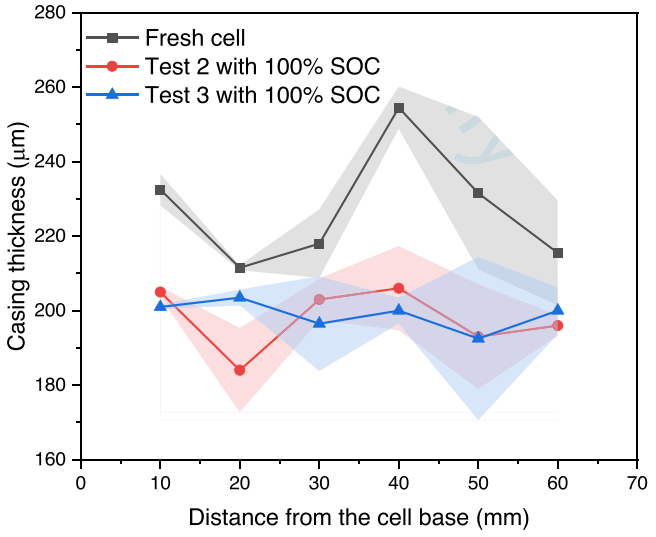

Figure 11. Comparison of battery casing thickness before and after the test. The shadowed area is the error bar of casing thickness.

in test 2 at the same SOC as shown in Fig. 10a, but the cavity in this test seems to be bigger than that in test 2 may be due to a bigger opening in this test. Cracks were not observed around the nail tip in this test. The other characteristics were similar to test 2 with 100% SOC.

Figure 11 shows a direct comparison of battery casing thickness with different distances from the cell base before and after the test. The error bar with fill area of casing thickness is plotted in Fig. 11. The thickness value in Fig. 11 is the mean value of two measurements at the same height but in different locations via a CT scan with

a resolution of 31 μm. The thickness of the cell at different locations after nail penetration test was less than that of the fresh cell, in other words, the thickness became thinner than the fresh cell. The average thicknesses of the fresh cell, test 2 and test 3 at different locations were 227 ± 16 μm, 198 ± 9 μm, and 199 ± 4 μm, respectively. It means that the battery casing thickness has been reduced by 12.7% ± 0.3% of the fresh cell. It may be caused by melt of the battery casing under high temperature. The cylindrical cell can be considered as a cylindrical pressure vessel. According to the stress analysis of the pressure vessels,[42] the hoop stress subjected to the cell thickness of the tested cell is 1.15 times that of the fresh cell. It suggests that the strength of the battery casing becomes weaker than that of the fresh cell due to thinner casing thickness. It may conduce to the occurrence of sidewall rupture.

Battery pack manufacturers intend to avoid sidewall rupture during TR, because it may cause catastrophic TR propagation between cells and even between battery modules. The reason and factors for sidewall rupture in these tests are as follows. The decrease of casing material in strength under high temperature is the main reasons for sidewall rupture. The hoop stress subjected to the cell increases due to the reduction of casing thickness under high temperature because the hoop stress is inversely proportional to casing thickness.[42] The tensile strength of the casing material at 800 °C dropped to 5% of that at room temperature as reported by Lao et al.[8] Therefore, the casing material becomes very weak under high temperature, which exceeds 800 °C for maximum surface temperature in some tests at high SOC. Another main reason is the huge increase in internal pressure, which is caused by a large volume of gases released during TR. Although the exact value of internal pressure in these tests is not known, it usually exceeds the venting pressure. The opening area of the venting disk and SOC also are important factors for sidewall rupture. The sidewall rupture will become easier if the safety valve does not work or is partly or completely blocked by broken electrode materials in tests. The cells at high SOC rupture easier than those at low SOC. In addition, the shock caused by nail movement may damage the outer casing of the cell. Sidewall rupture happened without TR, as highlighted in test 16 with 25% SOC. However, this condition was observed in only one test. Note that the sidewall rupture of the cell is also influenced by the penetrating depth of the nail, the nail speed, the diameter of the nail and the penetrating location which will be extensively studied in future tests, but not focused on here. Overall, sidewall rupture is mainly influenced by the casing strength under high temperature, the internal pressure, and the effective opening area of the venting disk. The internal pressure is also dependent on the SOC and the cell temperature, which is positively related to the SOC.

Suggestions in battery safety design.—According to the above analysis, an increase of the casing strength, the opening area of the venting disk and a decrease of the internal pressure and the SOC are effective measures to reduce the likelihood of sidewall rupture. However, the internal pressure is influenced by many factors in addition to the SOC and the cell temperature. Therefore, it is not an effective way to put it into action in battery safety design. The SOC of the cell is likely to change from very high to very low during operation. Therefore, worst case scenario should be used in battery safety design, i.e. 70%–100% SOC. However, SOC can be adopted as an indicator to assess the likelihood of sidewall rupture, for example, a cell less than 50% SOC suggests a low likelihood of sidewall rupture. Adopting alternative casing materials is one way to increase its strength at high temperatures, but at the same time, the material should have excellent chemical resistance and corrosion protection, desirable to be lightweight and low cost. An increase of casing thickness has been proved to be an effective way to prevent sidewall rupture, i.e. increasing the casing thickness from 0.22 mm to 0.30 mm.[8] However, this comes at the cost of weight, i.e. reducing the energy density of the cell.

For the cylindrical cells used in this work, there is only one venting disk located below the top over of the cell. More vents can provide more pathways to release pressure during TR. Some manufacturers have produced the cell with two vents, and one of them is located at the bottom of the cylindrical cell.[17,19] Although the effectiveness of preventing the sidewall rupture by designing two venting disks has not been verified and reported in the literature yet using this type of cells, it can be a safety measure to provide an extra pathway for gases release during TR because it is extremely important to relieve internal pressure in time avoiding the sidewall rupture. Overall, to reduce the possible sidewall rupture, increasing the casing thickness and adding the bottom vent are good practices in battery safety design to minimize the change of the cell. In addition, there are many ways to improve battery safety, interested readers can refer to Refs. 17, 19, 43, 44 for more details.

Conclusions

The behaviour of sidewall rupture of high specific energy 21700-format LIBs at different SOCs under radial nail penetration was studied. The main conclusions are as follows:

(1) The outcome of TR and sidewall rupture is more severe at high SOC ($\geqslant$ 50%) due to violent bursts of sparks and flame. 50% SOC was found to be the point at which the likelihood of sidewall rupture greatly increases. The sidewall rupture of the cell may occur below 50% SOC, but both the likelihood and the severity are low.
(2) The average mass loss increases with the increase of SOC.
(3) CT scans reveal a reduction in casing thickness, which may contribute to sidewall rupture of the cell. After analysing the main factors for sidewall rupture, it suggests that increasing the casing thickness/strength and adding the bottom vent are good practices in battery safety design to reduce the likelihood of sidewall rupture.

In addition, the current work provides a lot of details about temperature, voltage, mass, gases released, fire behaviour, and internal structure, which may be potentially used in the multi-physics modelling of cells under radial nail penetration. Note that the conclusions are made for 21700-format cells and are therefore not universal. But the above conclusions can provide a reference for analyzing the sidewall rupture behaviour of cylindrical cells under the similar testing conditions. To further understand the factors affecting sidewall rupture behaviour of LIBs, the effect of test parameters including nail diameter, nail speed, penetrating location, penetration depth, battery format, and battery chemistry on thermal runaway and sidewall rupture will be investigated in future work.

Acknowledgments

The research presented within this paper is supported by the Jaguar Land Rover Catapult project and the Faraday Institution "SafeBatt—Science of Battery Safety" [FIRG028]. The research was undertaken in collaboration with the WMG Centre High Value Manufacturing Catapult (funded by Innovate UK) and Jaguar Land Rover. The authors would like to acknowledge the help and support from Guillaume Remy for the CT scan from WMG at the University of Warwick. The X-ray CT was done in the National Facility for X-ray Computed Tomography (NXCT) and the Centre for Imaging, Metrology, and Additive Technologies (CiMAT) at the University of Warwick.

ORCID

Haodong Chen https://orcid.org/0000-0003-1295-6723

References

1. P. Sun, R. Bisschop, H. Niu, and X. Huang, *Fire Technol.*, **56**, 1361 (2020).
2. X. Feng, M. Ouyang, X. Liu, L. Lu, Y. Xia, and X. He, *Energy Storage Mater.*, **10**, 246 (2018).
3. Q. Wang, B. Mao, S. I. Stoliarov, and J. Sun, *Prog. Energy Combust. Sci.*, **73**, 95 (2019).

4. P. T. Coman, E. C. Darcy, C. T. Veje, and R. E. White, *Appl. Energy*, **203**, 189 (2017).
5. X. Feng, X. He, M. Ouyang, L. Lu, P. Wu, C. Kulp, and S. Prasser, *Appl. Energy*, **154**, 74 (2015).
6. X. Feng, J. Sun, M. Ouyang, F. Wang, X. He, L. Lu, and H. Peng, *J. Power Sources*, **275**, 261 (2015).
7. Z. Y. Jiang, Z. G. Qu, J. F. Zhang, and Z. H. Rao, *Appl. Energy*, **268**, 115007 (2020).
8. L. Lao, Y. Su, Q. Zhang, and S. Wu, *J. Electrochem. Soc.*, **167**, 090519 (2020).
9. F. Larsson, J. Anderson, P. Andersson, and B. E. Mellander, *J. Electrochem. Soc.*, **163**, A2854 (2016).
10. C. F. Lopez, J. A. Jeevarajan, and P. P. Mukherjee, *J. Electrochem. Soc.*, **162**, A1905 (2015).
11. G. B. Zhong, H. Li, C. Wang, K. Q. Xu, and Q. S. Wang, *J. Electrochem. Soc.*, **165**, A1925 (2018).
12. A. O. Said, C. Lee, and S. I. Stoliarov, *J. Power Sources*, **446**, 227347 (2020).
13. A. O. Said, C. Lee, S. I. Stoliarov, and A. W. Marshall, *Appl. Energy*, **248**, 415 (2019).
14. J. Weng, Y. He, D. Ouyang, X. Yang, M. Chen, S. Cui, G. Zhang, R. K. K. Yuen, and J. Wang, *Appl. Therm. Eng.*, **195**, 117147 (2021).
15. P. Huang, P. Ping, K. Li, H. Chen, Q. Wang, J. Wen, and J. Sun, *Appl. Energy*, **183**, 659 (2016).
16. V. Ruiz, A. Pfrang, A. Kriston, N. Omar, P. Van den Bossche, and L. Boon-Brett, *Renew. Sustain. Energy Rev.*, **81**, 1427 (2018).
17. B. Xu, J. Lee, D. Kwon, L. Kong, and M. Pecht, *Renew. Sustain. Energy Rev.*, **150**, 111437 (2021).
18. D. P. Finegan et al., *Adv Sci (Weinh)*, **5**, 1700369 (2018).
19. N. Anderson, M. Tran, and E. Darcy, *in Proc. S&T Meeting*p. 1 (2016).
20. D. P. Finegan et al., *Energy Environ. Sci.*, **10**, 1377 (2017).
21. L. Kong, X. Hu, G. Gui, Y. Su, and M. Pecht, *Fire Technol.*, **56**, 2565 (2020).
22. Y.-L Zhu, C.-J Wang, F. Gao, M.-X Shan, P.-L Zhao, Q.-F Meng, and Q.-B Wu, *Journal of Energy Storage*, **38**, 102571 (2021).
23. S. Doose, W. Haselrieder, and A. Kwade, *Batteries*, **7**, 6 (2021).
24. B. Liu, S. Yin, and J. Xu, *Appl. Energy*, **183**, 278 (2016).
25. B. Mao, H. Chen, Z. Cui, T. Wu, and Q. Wang, *Int. J. Heat Mass Transf.*, **122**, 1103 (2018).
26. J. Wang, W. Mei, Z. Cui, D. Dong, W. Shen, J. Hong, H. Chen, Q. Duan, Q. Wang, and J. Sun, *J. Therm. Anal. Calorim.*, **145**, 3255 (2021).
27. T. Yokoshima, D. Mukoyama, F. Maeda, T. Osaka, K. Takazawa, S. Egusa, S. Naoi, S. Ishikura, and K. Yamamoto, *J. Power Sources*, **393**, 67 (2018).
28. R. Zhao, J. Liu, and J. Gu, *Energy*, **123**, 392 (2017).
29. T. Ma, L. Chen, S. Liu, Z. Zhang, S. Xiao, B. Fan, L. Liu, C. Lin, S. Ren, and F. Wang, *J. Power Sources*, **437**, 7 (2019).
30. J. Xu, W. Mei, C. Zhao, Y. Liu, L. Zhang, and Q. Wang, *J. Therm. Anal. Calorim.*, **144**, 273 (2021).
31. D. P. Finegan, B. Tjaden, T. M. M. Heenan, R. Jervis, M. Di Michiel, A. Rack, G. Hinds, D. J. L. Brett, and P. R. Shearing, *J. Electrochem. Soc.*, **164**, A3285 (2017).
32. H. Chen, J. E. H. Buston, J. Gill, D. Howard, R. C. E. Williams, C. M. Rao Vendra, A. Shelke, and J. X. Wen, *J. Power Sources*, **472**, 228585 (2020).
33. H. Chen, J. E. H. Buston, J. Gill, D. Howard, R. C. E. Williams, E. Read, A. Abaza, B. Cooper, and J. X. Wen, *J. Electrochem. Soc.*, **168**, 010502 (2021).
34. A. W. Golubkov, S. Scheikl, R. Planteu, G. Voitic, H. Wiltsche, C. Stangl, G. Fauler, A. Thaler, and V. Hacker, *RSC Adv.*, **5**, 57171 (2015).
35. A. R. Baird, E. J. Archibald, K. C. Marr, and O. A. Ezekoye, *J. Power Sources*, **446**, 227257 (2020).
36. W. Li, H. Wang, Y. Zhang, and M. Ouyang, *J. Energy Storage*, **24**, 100775 (2019).
37. J. Diekmann, S. Doose, S. Weber, S. Munch, W. Haselrieder, and A. Kwade, *J. Electrochem. Soc.*, **167**, 10 (2020).
38. D. P. Finegan et al., *Nat. Commun.*, **6**, 6924 (2015).
39. T. Waldmann, R.-G. Scurtu, K. Richter, and M. Wohlfahrt-Mehrens, *J. Power Sources*, **472**, 228614 (2020).
40. X.-Y. Yao and M. G. Pecht, *IEEE Access*, **7**, 24082 (2019).
41. W. Zhao, G. Luo, and C.-Y. Wang, *J. Electrochem. Soc.*, **162**, A207 (2015).
42. D. Roylance, Pressure vessels in *Department of Materials Science and Engineering, Massachusetts Institute of Technology, Cambridge* (2001).
43. X. Feng, D. Ren, X. He, and M. Ouyang, *Joule*, **4**, 743 (2020).
44. Q. Wang, L. Jiang, Y. Yu, and J. Sun, *Nano Energy*, **55**, 93 (2019).